A Perspective for NREE

Inter-model consensus suggests 20th century ENSO likely influenced by climate change

Wenju Cai[1,2,3*], Benjamin Ng[3], Tao Geng[1,2], Fan Jia[4], Lixin Wu[1,2*], Guojian Wang[1,2,3], Yu Liu[5], Bolan Gan[1,2], Kai Yang[6], Agus Santoso[3,7], Xiaopei Lin[1,2], Yi Liu[2], Yun Yang[8], Fei-Fei Jin[9], Mat Collins[10], & Michael J. McPhaden[11]

[1]Laoshan Laboratory, Qingdao, China.

[2]Frontier Science Center for Deep Ocean Multispheres and Earth System and Key Laboratory of Physical Oceanography, Ocean University of China, Qingdao, China.

[3]Center for Southern Hemisphere Oceans Research (CSHOR), CSIRO Oceans and Atmosphere, Hobart, TAS, Australia.

[4]Key Laboratory of Ocean Circulation and Waves, Institute of Oceanology, Chinese Academy of Sciences, Qingdao, China.

[5]The State Key Laboratory of Loess and Quaternary Geology, Institute of Earth Environment, Chinese Academy of Sciences, Xi'an, China.

[6]State Key Laboratory of Numerical Modeling for Atmospheric Sciences and Geophysical Fluid Dynamics, Institute of Atmospheric Physics, Chinese Academy of Sciences, Beijing, China.

[7]Australian Research Council (ARC) Center of Excellence for Climate Extremes, , The University of New South Wales, Sydney, NSW, Australia.

[8]College of Global Change and Earth System Science, Beijing Normal University, Beijing China.

[9]Department of Atmospheric Science, SOEST, University of Hawaii at Manoa, Honolulu, Hawaii, USA.

[10]College of Engineering Mathematics and Physical Sciences, University of Exeter, Exeter, UK.

[11]NOAA/Pacific Marine Environmental Laboratory, Seattle, WA, USA.

*Correspondence to: Wenju Cai (Wenju.cai@csiro.au) or Lixin Wu (Lxwu@ouc.edu.cn).

Abstract

El Niño-Southern Oscillation (ENSO) sea surface temperature (SST) variability increased after 1960, accompanied by more frequent strong El Niño and La Niña events. Whether such changes are linked to anthropogenic warming is largely unknown, due to high natural variability and data limitations before the 1950s. In this Perspective, we examine the anthropogenic impact on changing ENSO variability using various experimental approaches with the latest climate model outputs. Overall, it is suggested that the observed post-1960 increase in ENSO variability has likely been influenced by greenhouse warming. Specifically, a comparison of simulated ENSO SST variability between 1901-1960 and 1961-2020 from a 'one experiment each model' approach indicates that approximately 77% of climate models produce an amplitude increase in post-1960 ENSO SST variability, translating into more frequent strong El Niño and La Niña events. Multiple large ensemble experiments further confirm that the simulated increase in post-1960 ENSO amplitude is not solely due to internal variability. Probability distribution of ENSO SST variability over 60-year periods using a multi-century-long simulation in 39 models under a constant pre-industrial CO_2 level also suggests that the observed post-1960 ENSO variability is high, sitting in the highest 2.5 and 10 percentiles for eastern- and central-Pacific ENSO, respectively. Improvement in model ENSO physics, assessment of consistent future and historical change in additional ENSO characteristics, and single-forcing large ensemble experiments will further ascertain the climate change impact on the observed ENSO.

Introduction

The El Niño-Southern Oscillation (ENSO)—the most consequential year-to-year fluctuation of the climate system(1Ropelewski1987;2Bove1998;3Bell1999;4McPhade2006;5Cai-ENSO-SA)—is characterized by two distinctive regimes(6Kug;7Kao;8Takahashi2011;9Takahashi2016;10Capotondi2015): eastern Pacific ENSO (EP-ENSO), wherein SST anomalies are centered in the equatorial eastern Pacific, with notably strong El Niño (warm) events in comparison to La Niña (cold) events; and central Pacific ENSO (CP-ENSO), wherein SST anomalies are centered in the central equatorial Pacific, with notably stronger La Niña events in comparison to El Niño. These changes in SST drive anomalous atmospheric convection, leading to large-scale reorganization of the Walker Circulation and shifts in the inter-tropical convergence zone(11Langaigne). As a result, ENSO is associated with considerable climate impacts, including El Niño-related droughts in western Pacific regions, floods in eastern Pacific countries(1Ropelewski;4McPhaden2006;5CaiENSO-SA), extreme swing of the South Pacific convergence zone toward the equator causing severe food shortage and cyclones to Pacific Island countries(12Cai2014;13Vincent;14Cai2012), and generally opposite impacts for La Niña. Beyond the tropical Pacific, long-term change in ENSO also affects Southern Ocean and Antarctic shelf ocean warming(15Wang2020NCC;16Cai2023NCC), changing the pace of Antarctic sea ice/ice sheet melt(17LiNREE2021).

Observations, aggregated across reanalysis products, suggest that ENSO variability might have changed over the course of the 20^{th} and 21^{st} centuries(18Zhang2008;19Kim2014;20Cai2021NREE). In particular, the E-index and C-index (representing indices for EP-ENSO and CP-ENSO, respectively) exhibit 32.3% (from 0.88 to 1.17) and 16.6% (from 0.96 to 1.12) increases in variance, respectively, when comparing 1901-1960 and 1961-2020 (Fig. 1a, b). The increase in E-index variability is associated with greater frequency of strong EP-El Niño events (from 2 events to 4 events) (Fig. 1c). By contrast, the increase in C-index variability reflects the greater frequency of strong La Niña years (from 1 event pre-1960 to 9 post-1960), with little change or a slight increase in the frequency of CP El Niño events (from 11 to 14 events) (Fig. 1d). The increase in ENSO variability is largely consistent across reanalysis datasets (Fig. 1e, f). Paleo-based analyses further suggest an increase in CP and EP-ENSO variability relative to the pre-industrial, including a ~25% intensification of over-arching ENSO variability during the late twentieth century relative to the pre-industrial period or distant before(21Grothe;22McGregor2010; 23McGregor2013;24Cobb;25Karamperidou;26Liu;27Freund).

Thus, reanalysis and paleo-based analyses suggest anthropogenic greenhouse gas forcing might have already contributed to an increase in ENSO variability. These changes are consistent with an consensus on projected SST variability increase(28CaiLaNiña; 20CaiENSOReview2021;29CaiNCCENSO-review;30CaiIPCC2022). However, determining the impact of anthropogenic warming on such changes in ENSO SST variability is hampered by uncertainty arising from decadal to multi-decadal fluctuations of ENSO, by low data quality before the 1950s due to sparse observations and sampling errors(31Kennedy), and by large uncertainties with paleo-reconstructions(32Gagan). Indeed, even if the observations are perfect in quality, the data are too short in length for an assessment of the possible internal variability range. Yet, determining the anthropogenic contributions to changing ENSO variability are vital to attribute causes of extreme events that are becoming more frequent and severe(33IPCC2021), to understand ENSO projection, and to gauge urgency of mitigation actions.

In this Perspective, we assess a possible impact by greenhouse warming on observed ENSO SST variability using three approaches with outputs from models participating in the sixth phase of Coupled Model Intercomparison Projects(34Eyring) (CMIP6) (Supplementary Information). Firstly, we use a 'one experiment each model' approach, referred to as 'model democracy' wherein only one experiment from each participating model is included in a multi-model ensemble assessment to quantify the change and multi-model consensus on ENSO change. Secondly, we use single model large ensemble experiments (separating uncertainty due to internal variability from that due to different model structures) to determine inter-experiment agreement and quantify changes after internal variability is removed. Thirdly, we use multi-century-long experiments under constant pre-industrial CO_2 forcing (piControl) to examine how unusual post-1960 ENSO variability is. The mechanisms underpinning an increase in post-1960 ENSO variability are subsequently discussed, before ending with an emerging picture on contemporary and future ENSO changes and recommendations for future research.

Consensus in 'one experiment each model' approach

Assuming that each model is independent and equally valid, the model democracy approach uses only one experiment from each model although many experiments could be available (Supplementary Information). Using one experiment only from each model avoids dominance by models with which many experiments are carried out such that each model is 'represented' equally in the assessment of inter-model consensus and the ensemble mean change. Here a total of 43 CMIP6 models are used each forced with observed historical emissions of greenhouse gases to 2014, and from the 2015 onward, under the Shared Socioeconomic Pathways 585(SSP585)(Ref.34Eyring). The full 120 years of 1901-2020 are divided into two longest possible equal-long 60-year subperiods. The longer the subperiods, the better the climate change signal is maximised and the influence of internal variability minimised(35Geng).

Using this approach, a strong inter-model consensus emerges on increased ENSO variability from the 20th to the 21st century in key characteristics of ENSO. These include an increased frequency of eastward propagating El Niño events(36Santoso2013), increased ENSO-related extreme rainfall variability even if ENSO SST variability does not change(12Cai2014;14Caietal2012;20Cai2021NREE;37Power-etal2013;38Wang-etal2020;39Brown2020;40Yun-et-al2021), increased SST variability in the equatorial central Pacific (Niño4 region) translating to an increased frequency of extreme La Niña(28CAILaNiña;41ENSObook), and enhanced EP-ENSO SST variability at anomaly centres unique to individual models(42Cai2018) in models with more realistic ENSO diversity and nonlinearity. The increased variability of EP- and CP-ENSO is associated with more occurrences of extreme EP El Niño and extreme La Niña events, and in swings from an extreme EP El Niño in a year to an extreme La Niña the next year(29Cai2015NCCReview). CMIP6 models have generally improved in this respect, and the projected increase in ENSO SST variability is simulated in a greater majority of models(43Fredriksen2020;20Cai2021). Using a conventional ENSO index, for example, Niño3.4 that represents CP- and EP-ENSO combined, an inter-model consensus on increased ENSO variability is simulated(30Cai2022).

Under this approach, a strong inter-model consensus emerges on stronger post-1960 ENSO variability than the pre-1960 period, with more frequent strong El Niño and strong La Niña events. A total of 33 out of 43 models combined (~77%) simulate an increase in standard deviation of the E-index, with a multi-model ensemble increase of 6.9±1.4% (Fig. 2a, b). A Bootstrap method (Supplementary Information) shows that the increase in E-index variability is statistically significant above the 95% confidence level. The increase in C-index standard deviation is 6.2±1.6%, supported by 27 out of 43 models (62.8%) generating an increase (Fig. 2c). In association, there is a multi-model average of 55.1% increase in the frequency of strong EP-El Niño events and a 59.7% increase in years of strong La Niña (Fig. 2d, e), both statistically significant; there is a slight decrease in CP-El Niño events that is not statistically significant. The strong inter-model consensus on the increase in post-1960 ENSO is also seen in Niño3.4 index (Supplementary Fig. 1).

Thus, the models under observed climate change forcing reproduce a post-1960 increase in E-index variability with an increased frequency of strong El Niño, and increased C-index variability with an increased frequency of strong La Niña, consistent with the projected change for the future climate(20Cai-NREE-Review;29CaiENSO-NCCreview;42Cai-EP-ENSO2018). The increased post-1960 variability is simulated even though each model has unique, independent internal variability different from the observed and from other models, in addition to other differences such as model physics. However, the inter-model spread is large ranging from -21.1% to 56.2% for E-index and from -22.1% to 56.7% for C-index, respectively, in terms of variability change in percentage. Internal variability is found to substantially impact on the spread in ENSO change under global warming(44Zheng;45Maher;46Wittenberg;47Stevenson;48NG;49Caibutterfly). It is therefore important to assess the inter-model difference after internal variability is removed.

Consensus in butterfly-effect large ensemble experiments

The large spread in the 'model democracy' approach confounds uncertainties from different sources(50Hawkins2009;51Deser2020) including model structure that determines climate sensitivity and internal variability from natural processes that operate even without climate change forcing. The uncertainty due to internal variability can be removed by creating a large ensemble simulations with each climate model under identical climate change forcing through an infinitesimal perturbation to the initial condition of each experiment (Supplementary Information). The perturbation creates diverging, randomly phased, and independent trajectories of ENSO(52Deser2012;53Hawkins2016;54Machete2016;55Bengtsson2019). As such, the forced change can be quantified by averaging over the experiments to remove the influence from internal variability, and assessed for an inter-experiment consensus. Seven available CMIP6 large ensemble experiments are used from models with at least 10 experiments and initiated from a time before 1900 and under historical forcing to 2014 (Supplementary Table 1); for the 2015-2020 period and beyond, an emission scenario in each model is chosen that provides the largest number of experiments.

Previous studies have found that the range of ENSO variability change could be as large as the entire range in the 'model democracy' spread of changes in CP-ENSO, EP-ENSO and their skewness between the 20th century and 21st century(44Zheng;45Maher;48Ng;49Cai), or more than 80% of the spread using two 30-year periods to depict the projected change(45Maher). Even in a multi-century-long experiment without external forcing, ENSO variability can be vastly different(46Wittenberg). That internal variability could confound the projected change is illustrated in a case in which the 'model democracy' approach produces no inter-model consensus but removing the impact of internal variability in each participating models through averaging their respective butterfly-effect ensemble experiments generates an inter-model consensus and a statistically significant change(47Stevenson). To remove impact of internal variability, at least 30-40 members are needed when using two 30-year periods to depict the projected change(45Maher), decreasing to 15 experiments when two 50-year periods are used(44Zheng). Importantly the number of experiments required decreases with a longer period used to determine the change(46Wittenberg).

Should greenhouse warming have not had an impact, one would expect approximately 50% of the butterfly-effect experiments to simulate greater ENSO variability post-1960 than pre-1960. This expectation, however, differs substantially from the actual result in that 225 out of 282 (79.8%) of experiments produce an increase in E-index (Fig. 3a), unlikely to be due to chances. Multi-experiment averages for each model, each having the impact of internal variability removed, show a strong inter-model consensus (Fig. 3b). These features are seen in C-index variability (Fig. 3c, d,) or in Niño3.4 variability (Supplementary Fig. 2), with 75.5% and 82.3% of experiments generating an increase, respectively. From the multi-experiment averages in the respective individual models, a multi-model mean E-index and C-index in each period is calculated for each period. The difference shows a mean increase of 10.6% and 8.3% in E-index and C-index, greater than a 6.9% and 6.2% increase, respectively, in the 'model democracy' approach. The inter-model range is 0.7-20.4% for E-index and 4.2-15.0% to 1for C-index, far smaller than that from the equivalent of the seven models in the 'model democracy' approach of 2.4-56.2% for E-index and 3.9- 44.4% for C-index, respectively. Thus, higher ENSO variability post-1960 than pre-1960 seen in the 'model democracy' approach is in part contributed by climate change.

Higher post-1960 ENSO variability relative to the pre-industrial level

Another approach to assess impact of greenhouse warming on ENSO is to determine if ENSO emerges from a probability distribution in a baseline period without influence of greenhouse warming(56Ying;35Geng). In effect, the baseline distribution, referred to as 'noise', measures range of natural fluctuations due to internal variability, and is compared to ENSO in a specific period to assess how unusual ENSO variability is or whether a signal emerges permanently out of the range of the noise(50Hawkins) (Supplementary Information). The distribution is diagnosed from multi-century-long piControl experiments(56Ying;35Geng). In CMIP6, outputs of long piControl simulation with at least 300 years are available from 39 climate models participating in the 'model democracy' approach and these are used for evaluating how unusual the observed post-1960 ENSO is (Supplementary Table 2). In total, there are 25,868 years of virtual climate that are used to construct the distribution of ENSO variability over 60-year periods.

To date, the consensus from this approach is that greenhouse warming-induced changes in tropical Pacific mean temperature and mean rainfall, or in variability of ENSO SST and rainfall, is uncertain and vastly different across models, with a large inter-model spread due to uncertainty in both signal and variability(56Ying;35Geng). However, changes in mean SST of the equatorial Pacific emerge earlier than in mean rainfall(56Ying). In contrast, changes in ENSO rainfall variability are projected to emerge earlier than changes in ENSO SST variability(20Caietal;56Ying). Specifically, using a 30-year period to diagnose signal and noise, approximately 70% of models simulate emergence before 2100, with a multi-model ensemble mean of ENSO rainfall variability signal emerging at about 2040 regardless of emission scenarios, some 30 years earlier than ENSO SST variability signal at about 2070(56Ying). In terms of ENSO SST variability in a 60- to 80-year range under the SSP585 emission scenario, increased EP-ENSO SST variability emerges around 2030 in ~70% of models, more than a decade earlier than that of CP-ENSO(35Geng). The earlier emergence of EP-ENSO results from an increase in EP-ENSO rainfall response(12Cai2014;14Cai2012;37Power2013), which boosts the signal of increased SST variability and is enhanced by an ENSO positive nonlinear atmospheric feedback(35Geng). The nonlinear Bjerknes feedback operates mainly in the eastern equatorial Pacific, in which once atmosphere deep convection is established, zonal winds increase nonlinearly with further increase in warming(9Takahashi2016;42Cai2018;57Geng2019;58Geng2020).

Measured against the distribution without greenhouse warming, the post-1960 ENSO variability is unusually high whereas the pre-1960 ENSO is not (Fig. 4). From the distribution of ENSO variability over 60-year periods, the highest 10, 5 and 2.5 percentile values of ENSO variability are identified. The amplitude of the observed post-1960 E-index variability is within the highest 2.5 percentile (Fig.4a), in a sharp contrast to the pre-1960 E-index variability amplitude, which sits around the 50th percentile. The observed amplitude of the post-1960 C-index variability sits between the highest 10 to top 5 percentiles for C-index (Fig.4b), which is also unusual but less so than the E-index, consistent with the finding that signal of ENSO change is more prominent in E-index than C-index(42CaiEastsernPacificNature;35Tao2022). Similarly, the amplitude of the observed pre-1960 C-index variability sits within around the 50th percentile. These features are seen using conventional ENSO index. The amplitude of the observed post-1960 Niño3.4 is unusually high setting within the highest 5 to 10 percentile (Supplementary Fig. 3). The high amplitude of post-1960 ENSO variability further supports that climate change has likely contributed to the observed ENSO increase.

Increased ENSO variability underpinned by intensified ocean stratification

Collectively the findings indicate a post-1960 increase in ENSO variance. In this section we show that the mechanism is similar to that responsible for the projected future ENSO change, namely changes in ocean stratification. In response to increasing emissions of greenhouse gases, an enhanced mean vertical stratification in the equatorial Pacific upper ocean occurs(59Collins;29CaiNCCENSOreview;42CaiEasternP-ElNiño), as the near-surface ocean warms faster than the ocean below. The faster near surface warming is a result of an increasing greenhouse-gas-induced radiative forcing and freshening from increased precipitation, which enhances the response of the surface mixed layer to a given wind forcing(42CaiEasternPacific;60Carreric;61Dewitte;62Thual), strengthening the ocean-atmosphere coupling(42CaiEasternPacif). The increased coupling contributes to a greater sensitivity of tropical Pacific SSTs to forcing from extratropical Pacific variability, such as the north Pacific meridional mode even though its own variability does not change(63Jia).

The increased coupling underpins the projected 21st century increase ENSO SST variability relative to the 20th century, and the projected increase in ENSO SST variability is independent of change in the surface west-minus-east SST gradient(42Cai-easternPacific). Although a faster warming in the eastern than the western equatorial Pacific tends to be associated with a greater increase in ENSO SST variability, and vice versa(64Zheng;65Hayashi;66Ying), the faster warming in the east in part results from a rectification of the increase in ENSO SST variability onto the mean state(65Hayashi;67Kohyama).

From the pre- to the post-1960 period, there is an intensification of the equatorial Pacific upper-ocean stratification that underpins the simulated ENSO change (Fig. 5a, b, c) as a faster warming occurs near the surface than at the subsurface. Statistically significant inter-model relationships exist in changes between the two periods; a greater enhancement in the vertical stratification is associated with a greater increase in E-index variability (Fig. 5a), which systematically translates into an increase in the frequency of strong El Niño (Fig. 5b). Because a strong El Niño causes a large heat discharge, shallowing of the central Pacific thermocline that is conducive to La Niña, the increase in the frequency of strong El Niño is in turn leads to more frequent strong La Niña events (Fig. 5d). The increase in the frequency of strong La Niña events contributes to an enhancement in C-index variability (Fig. 5e) despite the small reduction in central Pacific El Niño. Long-term observations of upper ocean temperatures are sparse and uncertain. There are two reanalysis datasets (68Balmaseda2008; 69Balmaseda2013) (Supplementary Information), in which vertical ocean temperatures date back to the 1950s. Equatorial Pacific temperatures averaged over the two products show an enhancement in vertical stratification, somewhat similar to the modelled (Fig. 5f). The similarity suggests that the mechanism identified in models for the post-1960 and future ENSO increase is likely at work.

Marching toward projected ENSO enhancement

That climate change has already enhanced ENSO variability consistent with the projected change means that the post-1960 increase is integral to the projected ENSO change. Since 1960, increasing CO_2 is not the only climate change forcing factor; emissions of sulphur aerosols have increased and then decreased back to the 1960 level. The decreased aerosol emissions in the latter part accelerated the warming of the post-1960 period(70IPCC2013), despite a continuous increase in emissions of other species that offset warming such as organic carbon or increase warming such as black carbon(71Hoesly2018). Butterfly-effect ensemble experiments under a single factor of forcing that separates the effect of changing aerosols from increasing CO_2, though available in two models only, suggest that overall changing aerosols have contributed to an increase in post-1950 ENSO variability(72Maher). The increasing CO_2 has a greater impact but the decreasing aerosols reinforced the conducive impact of increasing CO_2, and such an superimposing effect will continue into the future.

Going to the 60 years ending at 2100, a majority of the 43 models in the 'model democracy' approach show a further increase in amplitude of E-index, C-index and other indices under the SSP585 scenario (Supplementary Fig. 4). Comparisons of histograms of ensemble mean ENSO variability values over 60-year periods in the piControl experiments, in the 1961-2020 and the 2041-2100 period, show progressively increasing EP-ENSO towards the 2041-2100 period (Fig. 6a, b); by comparison, a further increase in CP-ENSO from the 1961-2022 level is smaller (Fig. 6c, d), reinforcing that change in EP-ENSO variability continues to be more detectable going into future(35Geng). The associated evolution of frequency of strong El Niño and strong La Niña, averaged across all models, shows a general long-term increasing trend into 2100 (Fig. 6b, d). The increasing trend is not linear, likely modulated by factors including ENSO-rectified mean state fluctuations(20Cai2021Review;65Hayashi) and a differential mean warming rate between ocean basins(19Kim).

The march toward projected ENSO enhancement seen in the 'model democracy' approach, may still be subject to residual influence of internal variability, particularly for C-index due to its weaker signal of increase. Importantly, the continuous increase in ENSO variability into the future is seen in multi-experiment means of the butterfly-effect ensembles, in which impact of internal variability is essentially removed; despite under different emission scenarios, six out of seven ensemble means show a continuous increase into the 2041-2100 period in E-index variability (Fig. 6e) and in Niño3.4 variability (Supplementary Fig. 5), and all seven models display an increase in C-index variability (Fig. 6f). The continuous increase reinforces that the post-1960 ENSO enhancement is likely a part of the long-term change.

Summary and future perspectives

In one single realization of the real world with limited observations, it is difficult, if not impossible, to determine whether observed ENSO has been affected by increasing emissions of greenhouse gases, even if quality of the available observation data is not an issue. Model outputs from multi-century-long simulations under the preindustrial level of constant CO_2 forcing, historical simulations under the observed forcing, and simulations of future climate under emission scenarios, offer a resource. The 'model democracy' approach shows that anthropogenic climate change has generated a statistically significant increase from the pre-1960 to the post-1960 level with a multi-model mean increase in ENSO SST variability in majority of climate models, featuring more frequent occurrences of strong El Niño and strong La Niña events in the post-1960 period, but little change in CP El Niño frequency. Many characteristics of the simulated changes appear in the observed change, although the similarity could be simply fortuitous. The simulated increase in post-1960 ENSO variability is seen in all seven models, in which large ensemble butterfly-effect experiments are conducted to remove impact of internal variability, supported by most experiments in each of the seven models. The observed ENSO variability on the post-1960 period appears unusually high compared to the distribution from 25,868 years of virtual climate of piControl experiments in 39 models. The simulated increase in post-1960 ENSO variability agrees with recent paleoclimatic evidence that ENSO variability in the 20th century and early 21st century is higher than in the distant past(21Grothe,23McGreger2013;26Liu2017) and is consistent with the projection that under future greenhouse warming ENSO SST variability will increase(28CaiLaNiña;42CaiEasternPacifucElNiño), underpinned by an intensified upper ocean stratification of the equatorial Pacific.

There are avenues to further ascertain the impact of climate change on the observed ENSO. Although dada quality issue of historical SST is perpetual, a continuous search for new ENSO proxies offers a potential to corroborate the findings based on existing ENSO proxies of a high post-1960 ENSO variability(21Grothe,23McGreger2013;26Liu2017). Any new proxies likely reflect a mixture of SST and hydroclimate signals rather than pure SST but would add to the weight of the available evidence. In terms of climate model assessment, examination of simulated future change in additional ENSO properties, for example, ENSO onset, termination, and seasonal phase locking, offers another pathway; a future change in any additional property of ENSO, if also seen in both the simulated and the observed post-1960 ENSO, would provide additional lines of evidence. Large ensemble of experiments under a single climate change forcing factor are currently available in limited number of models only(72Maher); given the effectiveness in reducing the inter-model spread and in quantifying the impact, such single-forcing large ensemble experiments performed in as many models as possible likely help separate the impact of CO_2, aerosols, and natural forcings such as volcanic eruptions, ultimately facilitating attribution of the post-1960 ENSO increase. Despite a substantial improvement from previous generations, most CMIP models still under-estimate ENSO nonlinear Bjerknes feedback(20Cai2021;30Cai2022IPCC), which amplifies ENSO response to greenhouse warming such that models simulate a greater feedback systematically generate a greater ENSO enhancement(35Geng2022;30Cai2022); improved parameterization of atmospheric convection, cloud formation and their coupling to ENSO processes(73Bony2005), leading to a realistic nonlinear Bjerknes feedback, potentially strengthens the simulated post-1960 ENSO enhancement and the inter-model consensus.

To conclude, the increase in observed ENSO variability during the post-1960 period, at least in part induced by anthropogenic climate change, is an integral part of the emerging increase in projected ENSO variability. The finding highlights the urgency of reducing greenhouse gas emissions to mitigate the adverse societal impacts of strong El Niño and strong La Niña events that are projected to continue to increase in the future.

Acknowledgments

This project is supported by the Science and Technology Innovation Project of Laoshan Laboratory (LSKJ202203300) and the Strategic Priority Research Program of Chinese Academy of Sciences (XDB 40030000). T.G. is supported by National Natural Science Foundation of China (NSFC) project (42206209) and China National Postdoctral Program for Innovative Talents (BX20220279). L.W., X.L., and B.G. are supported by the National Natural Science Foundation of China (NSFC) projects (41490643, 41490640, U1606402, and 41521091). W.C., G.W., B.N., and A.S. are supported by CSHOR, a joint research Center for Southern Hemisphere Oceans Research between QNLM and CSIRO. We acknowledge the World Climate Research Programme's Working Group on Coupled Modelling, which is responsible for CMIP, and we thank the climate modeling groups for producing and making available their model output. For CMIP the U.S. Department of Energy's Program for Climate Model Diagnosis and Intercomparison provides coordinating support and led development of software infrastructure in partnership with the Global Organization for Earth System Science Portals. We are grateful to various reanalysis groups for make the datasets available to us. PMEL contribution no. 4957.

Author contributions: W.C. conceived the article and wrote the initial manuscript in discussion with T.G., B.N. and L.W. B.N. and T. G. performed analysis and generated final figures. All authors contributed to interpreting findings, discussion of the associated dynamics, and improvement of this paper.

Competing interests: The authors declare no competing interests.

Data availability. Data relevant to the paper can be downloaded from website listed below:

- 20CRv2c at https://portal.nersc.gov/project/20C_Reanalysis/;
- CERA-20C at https://apps.ecmwf.int/datsets/dat/cera20c-edmo/levtype=sfc/type=an/;
- ERA-20C at https://apps.ecmwf.int/datsets/data/era20c-moda/levtype=sfc/type=an/;
- ERSST v3b at https://www.esrl.noaa.gov/psd/data/gridded/data.noaa.ersst.v3.html;
- HadISST v1.1 at https://www.esrl.noaa.gov/psd/data/gridded/data.hadsst.html;
- COBE at https://psl.noaa.gov/data/gridded/data.cobe.html;
- ORA-s3 at http://apdrc.soest.hawaii.edu/datadoc/ecmwf_oras3.php;
- ORA-s4 at https://climatedataguide.ucar.edu/climate-data/oras4-ecmwf-ocean-reanalysis-and-derived-ocean-heat-content;
- CMIP6 database at https://esgf-node.llnl.gov/projects/cmip6/

Code availability. Codes for calculating EOF can be downloaded from: https://drive.google.com/open?id=1d2R8wKpFNW-vMIfoJsbqIGPIBd9Z_8rj.

Figure Captions

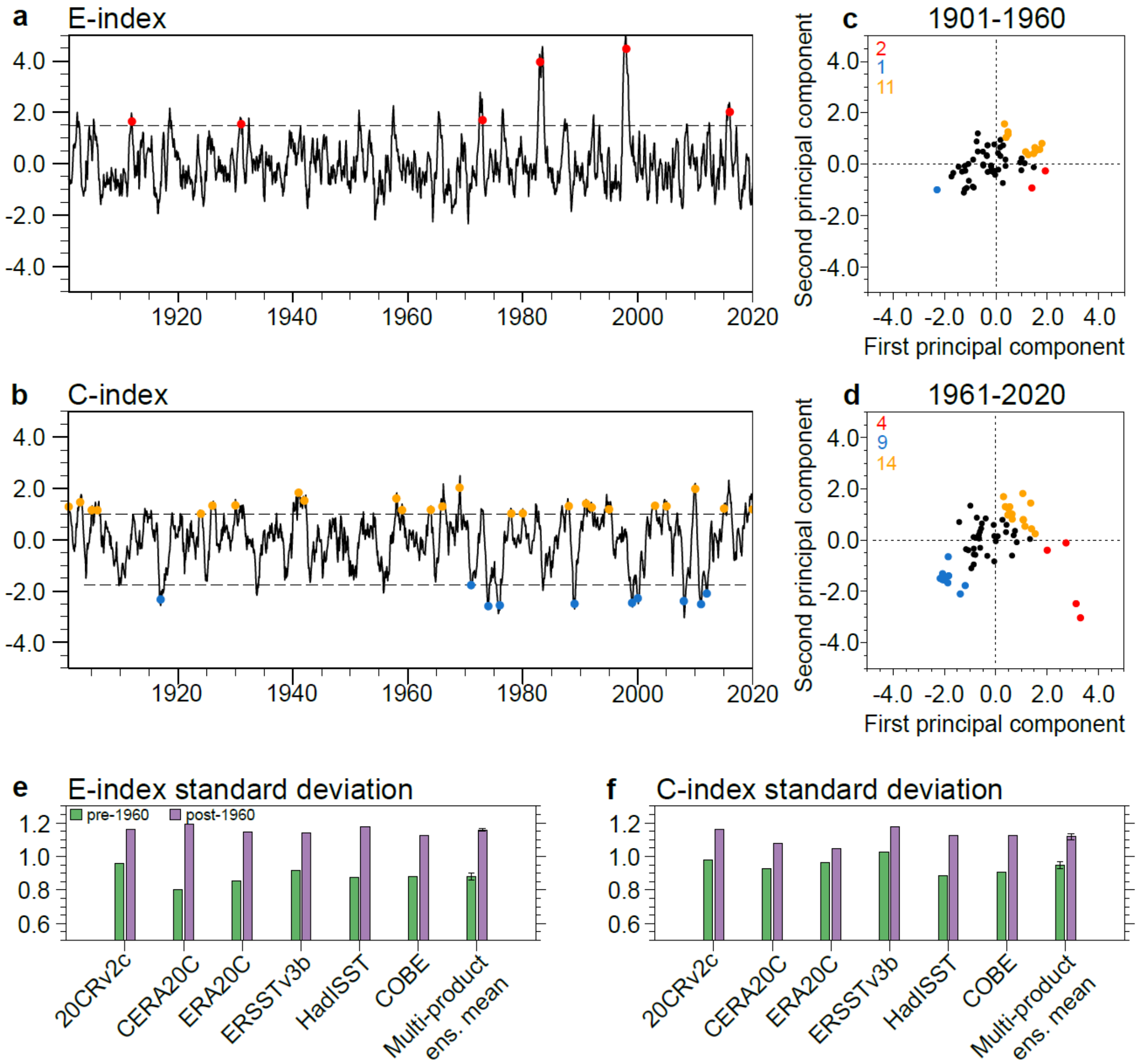

Fig. 1 | Observed E-index and C-index from 1901 to 2020. (**a, b**) | E-index and C-index time series averaged from six individual reanalysis datasets(74Compo2011;75Laloyaux2018;76Poli2016;77Smith2008;78Rayner2003;79Ishii2005), and (**c, d**) nonlinear relationship between the first and second principal component for the 1901 to 1960 period and the 1961 to 2020 period, respectively. The red dots indicate strong eastern Pacific El Niño events, defined as when the E-index averaged over December-February is greater than 1.5 standard deviation (s.d.), the orange dots indicate central Pacific El Niño events, defined as when the C-index is greater than 1.0 s.d., and blue dots denote strong La Niña events, defined as when the negative C-index has amplitude greater than 1.75 s.d., respectively. (**e, f**) | E-index and C-index standard deviation from six different reanalysis products, with the green and purple bars indicate the pre-1960 and post-1960 periods, respectively. The multi-product mean is the average of the standard deviations from the six products and the error bars represent the two standard deviation value of inter-product variability. Although there is an increase in ENSO variability, with only one realization, the possibility that the observed changes are due to internal variability cannot be excluded, even if data quality is not an issue.

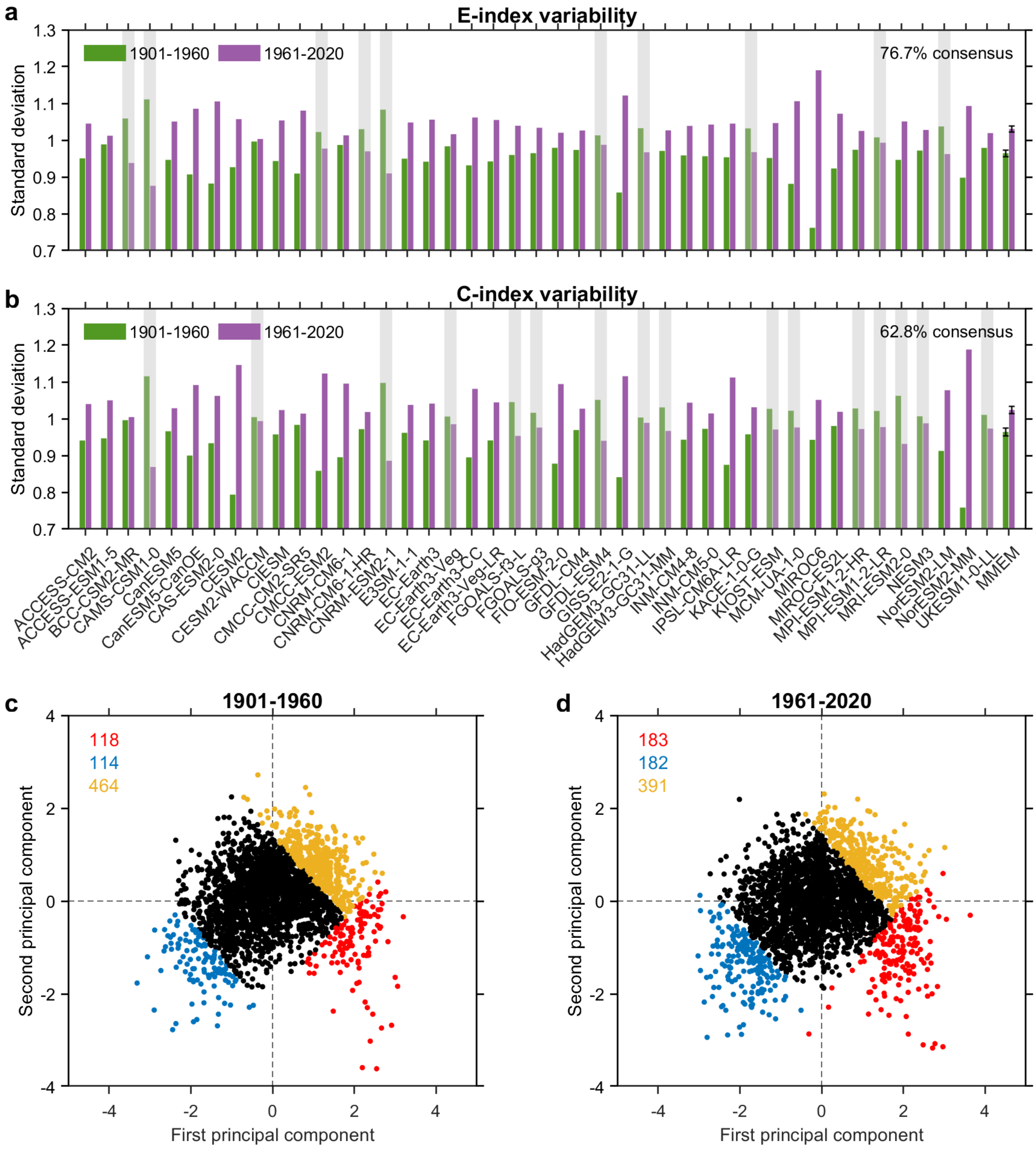

Fig. 2 | Simulated increase in post-1960 ENSO variability. (a, b) | E-index and C-index standard deviation (s.d.) for the 1901-1960 and 1961-2020 periods from 43 available CMIP6 models. The green and purple bars represent the 1901-1960 and 1961-2020 periods, respectively. The grey shading indicates models which do not simulate an increase in ENSO standard deviation. The percentage of models that simulate an increase is denoted on the top right. The range in the multi-model mean bars is defined as the two s.d. value of inter-model variability. (**c, d**) | Nonlinear relationship between the first and second principal components for the 1901 to 1960 period, and the 1961 to 2020 period, respectively. The blue, orange, and red dots indicate strong La Niña, central Pacific El Niño, and strong eastern Pacific El Niño events, respectively. The coloured numbers indicate the frequency of each type of event. Using one experiment each model, majority of models reproduce the observed increase in the post-1960 ENSO variability, featuring an increased frequency of strong El Niño and strong La Niña events.

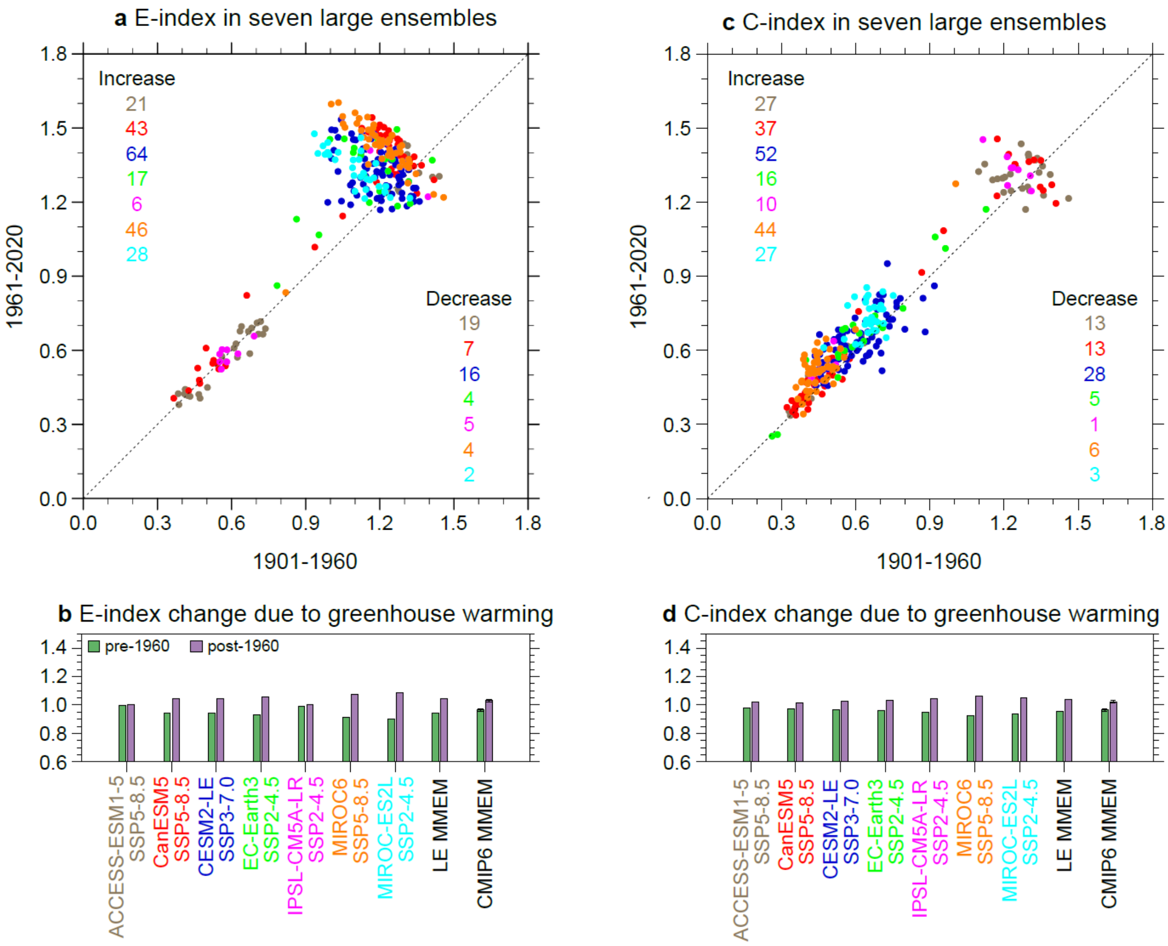

Fig. 3 | Increased post-1960 Niño3.4 variability in butterfly-effect ensembles of experiments. **a** | Pre-1960 (1901-1960) variability versus post-1960 (1961-2020) E-index variability for large ensembles in seven models. Number of experiments in each model producing an increase (decrease) in post-1960 ENSO variability is indicated in the top-left (bottom right) corner. Different SSPs are chosen to concatenate time series for the period of 2015-2020 to allow the largest number of experiments (Supplementary Table 1). **b |** Large ensemble mean E-index variability in the pre-1960 and the post-1960 60-year periods. The E-index for each ensemble experiment is standardised over the 1901-2020 period before calculating the ensemble average. The mean across the seven large ensemble averages is shown in the 2nd group of bars from right (LE MMEM) and the CMIP6 MMEM of the model democracy approach is also shown. The error bars represent the ±1.0 standard deviation range using a Bootstrap method. (**c, d**) | The same as (**a, b**) for for C-index). Without the influence from internal variability, all seven models generate an increase in ENSO variability post-1960.

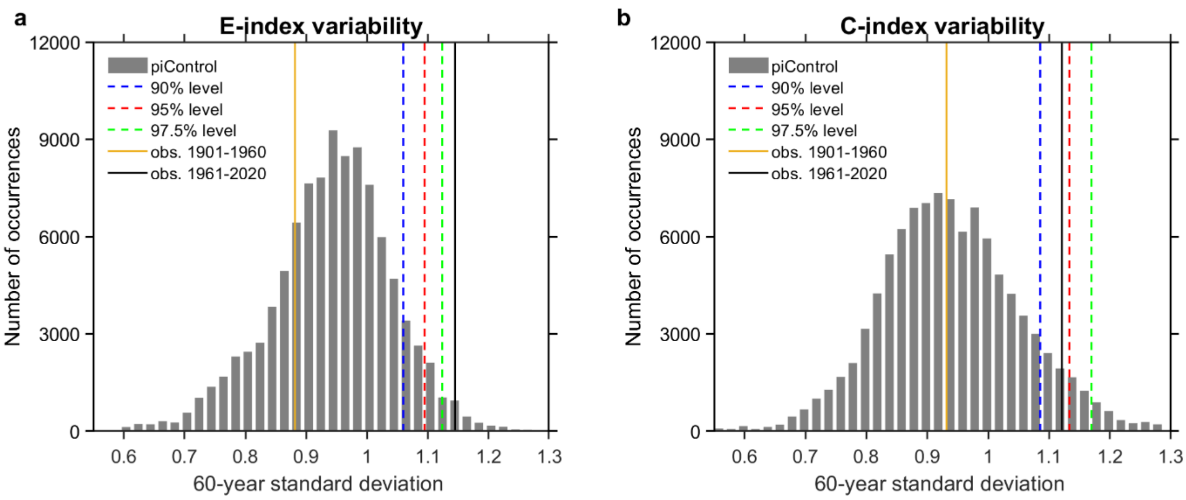

Fig. 4 | High variability of the post-1960 ENSO. **a** | Histogram (grey bars) of 100, 000 realizations of a Bootstrap method for 60-year running standard deviation (s.d.) of E-index in piControl from 39 CMIP6 models under a pre-industrial level of constant CO_2 with 25,868 years of virtual climate without climate change. The dashed blue, red and green lines indicate the upper 10, 5 and 2.5 percentile values of the histogram. Observed E-index variability (s.d.) in 1901-1960 and 1961-2020, averaged from multiple reanalysis datasets, are shown in solid brown and black lines, respectively. **b** | Same as **(a)** but for C-index. Compared to the distribution of ENSO variability over 60-year periods, the observed post-1960 ENSO amplitude is unusually high setting within the highest 2.5 and 10 percentile for E-index and C-index, respectively, in a sharp contrast to the pre-1960 ENSO, which sits below or around the 50 percentile.

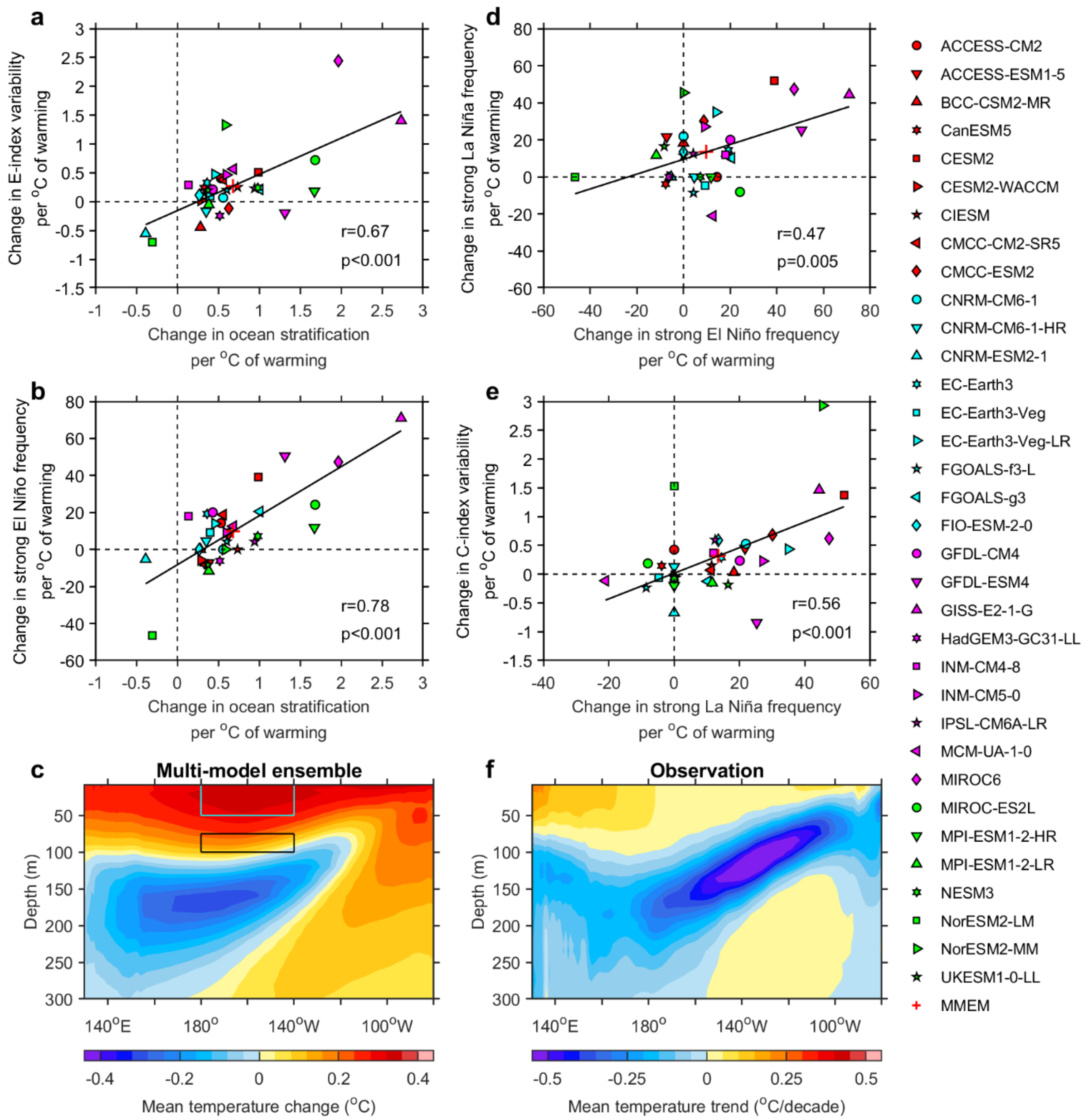

Fig. 5 | Changes in ocean stratification and in ENSO variability. (**a, b**) | Inter-model relationship between the change in ocean stratification and the change in (**a**) E-index standard deviation and in (**b**) frequency (events per 100 years) of strong El Niño events, for 34 CMIP6 models (symbols) in which ocean temperature data are available. Linear fit (solid black line) is displayed together with correlation coefficient *R* and corresponding *p* value. **c** | Multi-model ensemble averaged difference in mean ocean temperature warming between the 1961-2020 and 1901-1960 periods, from the 34 CMIP6 models; the light blue and black boxes indicate the regions used to calculate the change in ocean stratification in (**a**, **b**). **d** | Inter-model relationship between the change in frequency (events per 100 years) of strong El Niño events and the change in frequency (events per 100 years) of strong La Niña events. **e** | Inter-model relationship between the change in frequency (events per 100 years) of strong La Niña events and the change in C-index standard deviation. All changes in E-index, C-index, and ocean stratification have been scaled by the global sea surface temperature warming in each model between the two 60-year periods. **f** | Observed ocean temperature trend (ºC/decade) over the 1958 to 2017 period averaged from two reanalysis products (ORA-S3 and ORA-S4)(68Balmaseda2008; 69Balmaseda2013). Increased upper ocean stratification along the equatorial Pacific Ocean in the post-1960 period intensifies ocean-atmosphere coupling, leading to the simulated increase in the post-1960 ENSO amplitude.

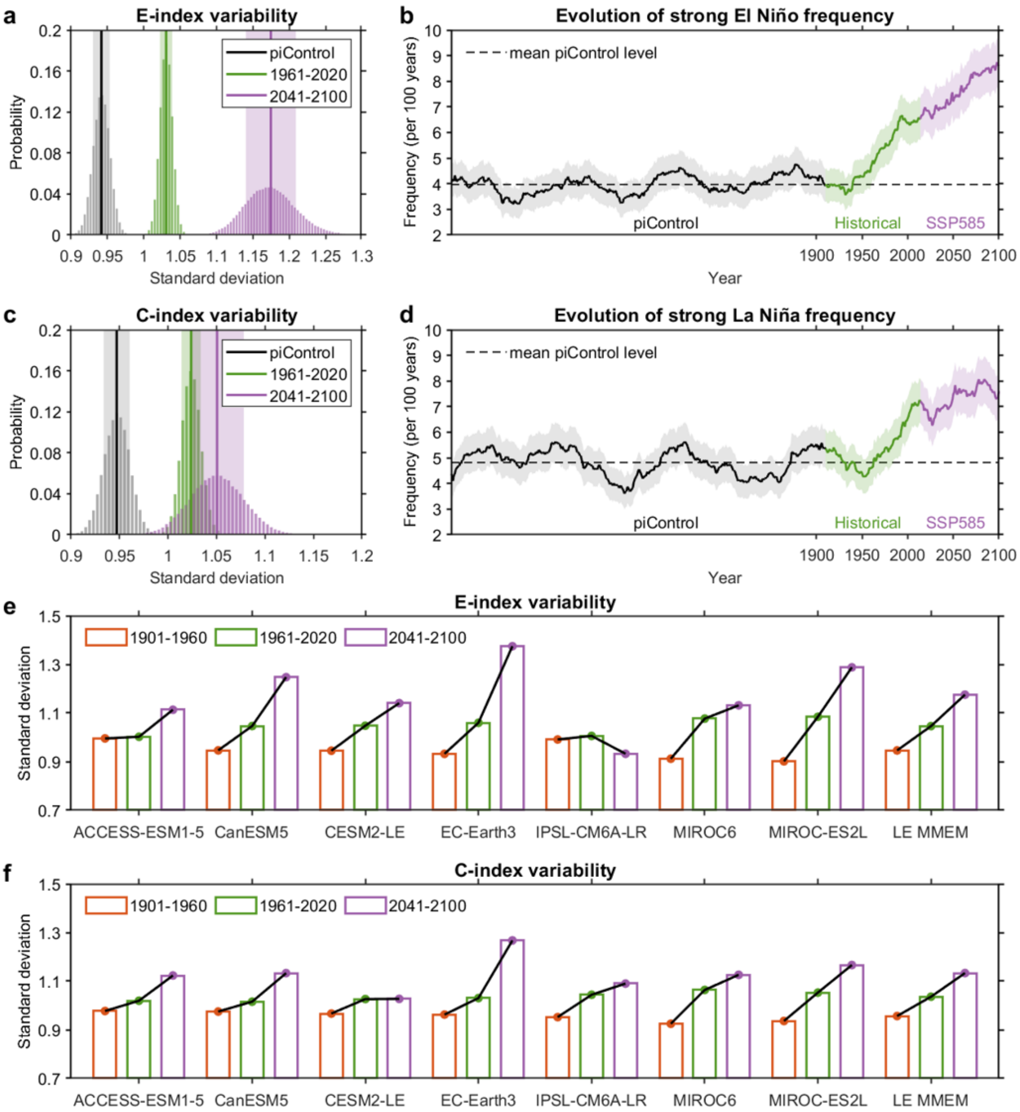

Fig. 6 | Continued increase of ENSO variability into the future. (**a**) | Histogram of 10, 000 realisations of 39-value ensemble means of a Bootstrap method on 60-year running standard deviation of E-index in piControl (gray bars), E-index standard deviation in the 1961-2020 (green bars) and the 2041-2100 (purple bars) periods, respectively, from the 39 CMIP6 models that have at least 300 years of piControl. Solid lines and shadings indicate multi-model mean and 1.0 s.d. of the 10,000 inter-realisations respectively. (**b**) | Evolution of strong El Niño frequency (events per 100 years) simulated over a period from piControl to 2100, diagnosed in 60-year sliding windows moving forward from the start of the last 300 years of piControl (black), covering the entire historical period till 2014 (green) and extending into the 21st century under a high-emission scenario SSP585 (purple). Solid lines and shadings indicate multi-model mean and 95% confidence intervals based on a Poisson distribution, respectively. The dashed black line indicates the mean level of piControl. (**c**, **d**) | Same as (**a, b**) but for C-index variability and strong La Niña frequency, respectively. (**e, f**) | Multi-experiment mean E-index and C-index standard deviation for the 1901-1960 (brown-edge bars), 1961-2020 (green-edge bars) and 2041-2100 (purple-edge bars) periods from each butterfly effect large ensemble (LE) experiments and the multi-model ensemble average (MMEM). ENSO variability progressively increases into the future, featuring an increasing frequency of strong El Niño and strong La Niña events.

References

1. Ropelewski, C. F. & Halpert, M. S. Global and regional scale precipitation patterns associated with the El Niño/Southern Oscillation. *Mon. Weath Rev.* **115**, 1606–1626 (1987).
2. Bove, M. C., Eisner, J. B., Landsea, C. W., Niu, X. & O'Brien, J. J. Effect of El Niño on U.S. landfalling hurricanes, revisited. *Bull. Am. Meteorol. Soc.* **79**, 2477-2482 (1998).
3. Bell, G. D. *et al.* Climate assessment for 1998. *Bull. Am. Meteorol. Soc.* **80**, 1040-1040 (1999).
4. McPhaden, M. J., Zebiak, S. E. & Glantz, M. H. ENSO as an integrating concept in earth science. *Science* **314**, 1740-1745 (2006).
5. Cai, W. *et al.* Climate impacts of the El Niño-Southern Oscillation on South America. *Nat. Rev. Earth Environ.* **1**, 215-231 (2020).
6. Kug, J. S., Jin, F. F. & An, S. Il. Two types of El Niño events: Cold tongue El Niño and warm pool El Niño. *J. Clim.* **22**, 1499-1515 (2009).
7. Kao, H. Y. & Yu, J. Y. Contrasting eastern-Pacific and central-Pacific types of ENSO. *J. Clim.* **22**, 615-632 (2009).
8. Takahashi, K., Montecinos, A., Goubanova, K. & Dewitte, B. ENSO regimes: reinterpreting the canonical and Modoki El Niño. *Geophys. Res. Lett.* **38,** L10704 (2011).
9. Takahashi, K. & Dewitte, B. Strong and moderate nonlinear El Niño regimes. *Clim. Dyn.* **46**, 1627-1645 (2016).
10. Capotondi, A. *et al.* Understanding ENSO diversity. *Bull. Am. Meteorol. Soc.* **96**, 921-938 (2015).
11. Lengaigne, M. & Vecchi, G. A. Contrasting the termination of moderate and extreme El Niño events in coupled general circulation models. *Clim. Dyn.* **35**, 299-313 (2010).
12. Cai, W. *et al.* Increasing frequency of extreme El Niño events due to greenhouse warming. *Nat. Clim. Chang.* **4**, 111-116 (2014).
13. Vincent, E. M. *et al.* Interannual variability of the South Pacific Convergence Zone and implications for tropical cyclone genesis. *Clim. Dyn.* **36**, 1881–1896 (2011).
14. Cai, W. *et al.* More extreme swings of the South Pacific convergence zone due to greenhouse warming. *Nature* **488**, 365-369 (2012).
15. Wang, G. et al., Future Southern Ocean warming linked to projected ENSO variability. *Nat. Clim. Chang.* **12**, 649-654 (2022).
16. Cai, W. *et al.* Antarctic shelf ocean warming and sea ice melf affected by projected El Niño

changes. *Nat. Clim. Chang.* https://doi.org/10.1038/s41558-023-01610-x (2023).

17. Li, X. et al., Tropical teleconnection impacts on Antarctic climate changes. *Rev. Earth. Environ*. **2**, 680-698 (2021).
18. Zhang, Q., Guan, Y. & Yang, H. ENSO amplitude change in observation and coupled models. *Adv. Atmos. Sci.* **25**, 361-366 (2008).
19. Kim, S. T. *et al.* Response of El Niño sea surface temperature variability to greenhouse warming. *Nat. Clim. Chang.* **4**, 786-790 (2014).
20. Cai, W. et al., Changing El Niño-Southern Oscillation in a warming climate. *Nat. Rev. Earth. Environ.* **2**, 628-644 (2021).
21. Grothe, P. R. *et al.* Enhanced El Niño-Southern Oscillation variability in recent decades. *Geophys. Res. Lett.* **47**, e2019GL083906 (2020).
22. McGregor, S., Timmermann, A. & Timm, O. A unified proxy for ENSO and PDO variability since 1650. Clim. Past. 6, 1-17 (2010).
23. McGregor, S., Timmermann, A., England, M. H., Elison Timm, O. & Wittenberg, A. T. Inferred changes in El Niño-Southern Oscillation variance over the past six centuries. *Clim. Past* **9**, 2269-2284 (2013).
24. Cobb, K. M. et al. Highly Variable El Niño-Southern Oscillation Throughout the Holocene. *Science* **339**, 67-70 (2013).
25. Karamperidou, C. et al. ENSO in a Changing Climate: Challenges, Paleo-Perspectives, and Outlook. *In El Niño Southern Oscillation in a Changing Climate (eds M.J. McPhaden, A. Santoso and W. Cai). AGU Monograph*, (2020).
26. Liu, Y. et al. Recent enhancement of central Pacific El Niño variability relative to last eight centuries. *Nat. Commun.* **8**, 15386 (2017).
27. Freund, M. et al. Higher frequency of Central Pacific El Niño events in recent decades relative to past centuries, *Nat. Geosci.* **12**, 450-455 (2019).
28. Cai, W. *et al.* Increased frequency of extreme La Niña events under greenhouse warming. *Nat. Clim. Chang.* **5**, 132-137 (2015).
29. Cai, W. *et al.* ENSO and greenhouse warming. *Nat. Clim. Chang.* **5**, 849-859 (2015).
30. Cai, W. *et al.* Increased ENSO sea surface temperature variability under four IPCC emission scenarios. *Nat. Clim. Chang.* **12**, 228-231 (2022).
31. Kennedy, J. J. A review of uncertainty in in situ measurements and data sets of sea surface teperature. *Rev. Geophys*. **52**, 1-32 (2014).
32. Gagan, M. K. Paleo-El Niño-Southern Oscillation (ENSO) Records. *Enclyclopedia Palaeoclimatol. Anc. Environ.* 721-728 (2009).

33. IPCC Climate Change 2021: The Physical Science Basis (eds Masson-Delmotte, V. et al.) (Cambridge Univ. Press, in the press).
34. Eyring, V. *et al.* Overview of the Coupled Model Intercomparison Project Phase 6 (CMIP6) experimental design and organization. *Geosci. Model Dev.* **9**, 1937-1958 (2016).
35. Geng, T. *et al.* Emergence of changing Central-Pacific and Eastern-Pacific El Niño-Southern Oscillation in a warming climate. *Nat. Commun* **13**, 6616 (2022).
36. Santoso, A. et al. Late-twentieth-century emergence of the El Niño propagation asymmetry and future projections. *Nature* **504**, 126 (2013).
37. Power, S. B., Delage, F., Chung, C., Kociuba, G., & Keay, K. Robust twenty-first century projections of El Niño and related precipitation variability. *Nature* **502**, 541-545 (2013).
38. Wang, G. et al. Continued increase of extreme El Niño frequency long after 1.5°C warming stabilization. *Nat. Clim. Change* **7**, 568-572 (2017).
39. Brown, J.R., Lengaigne, M., Lintner, B.R. *et al.* South Pacific Convergence Zone dynamics, variability and impacts in a changing climate. *Nat Rev Earth Environ* **1,** 530-543 (2020).
40. Yun, K. S. et al. Increasing ENSO-rainfall variability due to changes in future tropical temperature–rainfall relationship. *Commun. Earth Environ.* **2,** 43 (2021).
41. McPhaden, M. J., Santoso, A., & Cai, W. (Eds.). El Niño Southern Oscillation in a Changing Climate **253,** *John Wiley & Sons* (2020).
42. Cai, W. *et al.* Increased variability of eastern Pacific El Niño under greenhouse warming. *Nature* **564**, 201-206 (2018).
43. Fredriksen, H.-B., Berner, J., Subramanian, A. C., & Capotondi, A. How does El Niño-Southern Oscillation change under global warming-A first look at CMIP6. *Geophys. Res. Lett.* **47**, e2020GL090640 (2020).
44. Zheng, X. T., Hui, C. & Yeh, S. W. Response of ENSO amplitude to global warming in CESM large ensemble: uncertainty due to internal variability. *Clim. Dyn.* **50**, 4019-4035 (2018).
45. Maher, N., Matei, D., Milinski, S. & Marotzke, J. ENSO change in climate projections: forced response or internal variability? *Geophys. Res. Lett.* **45**, 390-398 (2018).
46. Wittenberg, A. T. Are historical records sufficient to constrain ENSO simulations? *Geophysical Research Letters* **36,** L12702 (2009).
47. Stevenson, S. L. Significant changes to ENSO strength and impacts in the twenty-first century: Results from CMIP5, *Geophys. Res. Lett.* **39**, L17703 (2012).

48. Ng, B., Cai, W., Cowan, T., & Bi, D. Impacts of Low-Frequency Internal Climate Variability and Greenhouse Warming on El Niño-Southern Oscillation, *J. Clim.* **34**, 2205-2218 (2021).
49. Cai, W. *et al.* Butterfly effect and a self-modulating El Niño response to global warming. *Nature* **585**, 68-73 (2020).
50. Hawkins, E. & Sutton, R. Time of emergence of climate signals. *Geophys. Res. Lett.* **39**, L01702 (2012).
51. Deser, C. *et al.* Insights from Earth system model initial-condition large ensembles and future prospects. *Nat. Clim. Change* **10**, 277-286 (2020).
52. Deser, C. *et al.* ENSO and Pacific decadal variability in the Community Climate System Model version 4. *J. Clim.* **25**, 2622-2651 (2012).
53. Hawkins, E., Smith, R. S., Gregory, J. M., & Stainforth, D. A. Irreducible uncertainty in near-term climate projections. *Clim. Dyn.* **46**, 3807-3819 (2016).
54. Machete, R. L., & Smith, L. A. Demonstrating the value of larger ensembles in forecasting physical systems. *Tellus A: Dynamic Meteorology and Oceanography*, **68**, 28393 (2016).
55. Bengtsson, L., & Hodges, K. I. Can an ensemble climate simulation be used to separate climate change signals from internal unforced variability? *Clim. Dyn.* **52**, 3553-3573 (2019).
56. Ying, J., Collins, M., Cai, W., Timmermann, A., Huang, P., Chen, D., & Stein, K. Emergence of climate change in the tropical Pacific. *Nat. Clim. Change* **12**, 356-364 (2022).
57. Geng, T., Cai, W., & Wu, L. Two types of ENSO varying in tandem facilitated by nonlinear atmospheric convection. *Geophys. Res. Lett.* **47**, e2020GL088784 (2020).
58. Geng, T., Cai, W., Wu, L., & Yang, Y. Atmospheric convection dominates genesis of ENSO asymmetry. *Geophys. Res. Lett.* **46**, 8387-8396 (2019).
59. Collins, M. *et al.* The impact of global warming on the tropical Pacific ocean and El Niño. *Nat. Geosci.* **3**, 391-397 (2010).
60. Carréric, A. et al. Change in strong Eastern Pacific El Niño events dynamics in the warming climate. *Clim. Dyn.* **54**, 901-918 (2020).
61. Dewitte, B., Yeh, S.-W., Moon, B.-K., Cibot, C. & Terray, L. Rectification of the ENSO variability by interdecadal changes in the equatorial background mean state in a CGCM simulation. *J. Clim.* **20**, 2002-2021 (2007).
62. Thual, S., Dewitte, B., An, S.-I. & Ayoub, N. Sensitivity of ENSO to stratification in a recharge–discharge conceptual model. *J. Clim.* **4**, 4331-4348 (2011).

63. Jia, F., Cai, W., Gan, B., Wu, L., & Di Lorenzo, E. Enhanced North pacific impact on El Niño/southern oscillation under greenhouse warming. *Nat. Clim. Change* **11**, 840-847 (2021).
64. Zheng, X.-T., Xie, S.-P., Lv, L. H. & Zhou, Z. Q. Intermodel uncertainty in ENSO amplitude change tied to Pacific Ocean warming pattern. *J. Clim.* **29**, 7265–7279 (2016).
65. Hayashi, M., Jin, F.-F. & Stuecker, M. F. Dynamics for El Niño-La Niña asymmetry constrain equatorial-Pacific warming pattern. *Nat. Commun.* **11**, 4230 (2020).
66. Ying, J., Huang, P., Lian, T. & Chen, D. Intermodel uncertainty in the change of ENSO's amplitude under global warming: role of the response of atmospheric circulation to SST anomalies. *J. Clim.* **32**, 369-383 (2019).
67. Kohyama, T., Hartmann, D. L. & Battisti, D. S. La Niña–like mean-state response to global warming and potential oceanic roles. *J. Clim.* **30**, 4207-4225 (2017).
68. Balmaseda, M. A., Vidard, A. & Anderson, D. L. T. The ECMWF ocean analysis system: ORA-S3. *Mon. Weath Rev.* **136**, 3018–3034 (2008).
69. Balmaseda, M. A., Mogensen, K. & Weaver, A. T. Evaluation of the ECMWF ocean reanalysis system ORAS4. *Q. J. R. Meteorol. Soc.* **139**, 1132–1161 (2013).
70. IPCC Climate Change 2013: The Physical Science Basis. Contribution of Working Group I to the Fifth Assessment Report of the Intergovernmental Panel on Climate Change [Stocker, T.F., Qin, D., Plattner, G.-K., Tignor, M., Allen, S.K., Boschung, J., et al. (eds.)]. Cambridge University Press, Cambridge, United Kingdom and New York, NY, USA, 1535 pp
71. Hoesly, R. M., et al. Historical (1750-2014) anthropogenic emissions of reactive gases and aerosols from the Community Emissions Data System (CEDS). *Geosci. Model Dev.,* **11**, 369-408 (2018).
72. Maher, N. *et al.* The future of the El Niño-Southern Oscillation: Using large ensembles to illuminate time-varying responses and inter-model differences. *Earth Syst. Dyn. Discuss.*, 1-28 (2022).
73. Bony, S. & Dufresne, J. L. Marine boundary layer clouds at the heart of tropical cloud feedback uncertainties in climate models. *Geophys. Res. Lett.* **32**, L20806 (2005).
74. Compo, G. P. *et al.* The twentieth century reanalysis project. *Quarterly Journal of the Royal Meteorological Society* **137**, 1–28 (2011).
75. Laloyaux, P. *et al.* CERA-20C: A coupled reanalysis of the twentieth century. *J. Adv. Model. Earth Syst.* **10**, 1172–1195 (2018).

76. Poli, P. *et al.* ERA-20C: An atmospheric reanalysis of the twentieth century. *J. Clim.* **29**, 4083–4097 (2016).

77. Smith, T. M., Reynolds, R. W., Peterson, T. C. & Lawrimore, J. Improvements to NOAA's historical merged land-ocean surface temperature analysis (1880-2006). *J. Clim.* **21**, 2283–2296 (2008).

78. Rayner, N. A. et al. Global analyses of sea surface temperature, sea ice, and night marine air temperature since the late nineteenth century. *J. Geophys. Res.* **108,** 4407 (2003).

79. Ishii, M., Shouji, A., Sugimoto, S., & Matsumoto, T. Objective Analyses of Sea-Surface Temperature and Marine Meteorological Variables for the 20th Century using ICOADS and the Kobe Collection. *Int. J. Climatol.*, **25**, 865-879 (2005).